Turing pattern dynamics in an activator-inhibitor system with superdiffusion

Lai Zhang*
Department of Mathematics and Mathematical Statistics, Umeå University, SE-90187, Umeå, Sweden

Canrong Tian†
Department of Basic Sciences, Yancheng Institute of Technology, Yancheng 224003, China

(Received 14 March 2014; revised manuscript received 20 November 2014; published 19 December 2014)

The fractional operator is introduced to an activator-inhibitor system to describe species anomalous superdiffusion. The effects of the superdiffusive exponent on pattern formation and pattern selection are studied. Our linear stability analysis shows that the wave number of the Turing pattern increases with the superdiffusive exponent. A weakly nonlinear analysis yields a system of amplitude equations and the analysis of these amplitude equations predicts parameter regimes where hexagons, stripes, and their coexistence are expected. Numerical simulations of the activator-inhibitor model near the stability boundaries confirm our analytical results. Since diffusion rate manifests in both diffusion constant and diffusion exponent, we numerically explore their interactions on the emergence of Turing patterns. When the activator and inhibitor have different superdiffusive exponents, we find that the critical ratio of the diffusion rate of the inhibitor to the activator, required for the formation of the Turing pattern, increases monotonically with the superdiffusive exponent. We conclude that small ratio (than unity) of anomalous diffusion exponent between the inhibitor and activator is more likely to promote the emergence of the Turing pattern, relative to the normal diffusion.

DOI: 10.1103/PhysRevE.90.062915 PACS number(s): 89.75.Kd, 87.23.−n, 05.45.−a, 82.39.−k

I. INTRODUCTION

Turingpattern formation describes the emergence of spatially inhomogeneous distributions of species density as a consequence of Turing instability or diffusion-driven instability. This scenario was first discovered by Turing [1] in a two species reaction-diffusion chemical system and since then Turing's idea has been quickly spread to other fields such as biology [2–4], physics [5,6], neuroscience [7], and optics [8,9]. As an interesting application in biology, Turing pattern formation in activator-inhibitor systems may be able to, from a theoretical point of view, explain the formation of animal coat patterns [10], and the occurrence of different clone patterns [11]. The standard two species reaction-diffusion model reads in the following form:

$$\begin{aligned} \frac{\partial u}{\partial t} &= \nabla^2 u + f(u,v), \\ \frac{\partial v}{\partial t} &= d\nabla^2 v + g(u,v), \end{aligned} \tag{1}$$

where u (activator) and v (inhibitor) represent the concentrations of two chemical species, respectively. $f(u,v)$ and $g(u,v)$ are reaction terms, whose specified forms depend on investigated systems. d is the diffusion ratio between the inhibitor and activator. For Turing patterns to form it is well known that the diffusion ratio must be sufficiently large (greater than unity).

The diffusion in system (1) is a depiction of standard Brownian motion, i.e., nearest jumps at the molecular level, and characterized by the fact that both waiting time distribution and jump size distribution must have finite moments. However, the particles do not necessarily always execute the nearest jumps, but instead they can wait between successive jumps and perform long jumps. When the conditions of finite moments in the distributions of waiting time and jump size are not met, particles undergo anomalous diffusion [12–17]. For convenience we denote the former diffusion by "normal diffusion". There are two types of anomalous diffusion, superdiffusion and subdiffusion. The superdiffusion, a diffusion process faster than normal diffusion, corresponds to a jump size distribution having infinite moments, or alternatively, Lévy flights [14]. It occurs in the processes of plasmas and turbulent flows [18,19], surface diffusion [20], and motion of animals [21–23]. The subdiffusion, a diffusion process slower than normal diffusion, corresponds to a waiting time distribution having infinite moments. It often occurs in gels [24], porous media [25], and polymers [26]. Both types of anomalous diffusion have been recognized to play an important role in biological, physical, and chemical processes.

Pattern formation in reaction-diffusion systems with anomalous diffusion has received considerable attention [16,17,27–31]. For instance, it was shown that subdiffusion suppresses the formation of the Turing pattern [31]. It was also found in one-dimensional systems that anomalous heat conduction can happen as a consequence of the anomalous diffusion [32]. Additionally, in systems with Lévy flights, the emergence of spiral waves and chemical turbulence from the nonlinear dynamics of oscillating reaction-diffusion patterns was investigated in [33]. In [16] the authors explored the effects of superdiffusion on pattern formation and pattern selection in the substrate-depleted Brusselator model [34]. They found that Turing instability can occur even when diffusion of the inhibitor is slower than that of the initiator. However, results on the nonlinear dynamics and Turing pattern selection in activator-inhibitor systems with superdiffusion remain unclear. To this end, we focus on pattern selection in the formation of hexagons and stripes and compare the cases of normal and

*Lai.Zhang@math.umu.se
†Corresponding author: tiancanrong@163.com

superdiffusion in the following activator-inhibitor model:

$$\begin{aligned}\frac{\partial u}{\partial t} &= \nabla^{\gamma} u + u - av + buv - u^3,\\ \frac{\partial v}{\partial t} &= d\nabla^{\gamma} v + u - cv,\end{aligned} \tag{2}$$

where the superdiffusion is described by the Weyl fractional operator ∇^{γ} $(1 < \gamma < 2)$. The fractional operator implies a heavy tailed random walk model with infinite variance of the particle jumps, where occasional large jumps dominate the more common smaller jumps. The type of particle jumps correspond to Lévy flights, which is observed in animals' hunting patterns (especially for ocean predators and birds) [35,36]. The fractional γ characterizes the heavy tail of particle jumps, say Y, that is, $P(|Y| > r) \approx r^{-\gamma}$ [37]. For $\gamma = 2$ the classic random walks following the Gaussian distribution are recovered.

In the case of $1 < \gamma < 2$, an extended central limit theorem due to Lévy [38] applies to show that the particle follows a stable density curve (see, for example, [39–41]), the solution to a fractional diffusion equation

$$\frac{\partial v}{\partial t} = d\nabla^{\gamma} v. \tag{3}$$

In one dimension, the fractional operator is written in the form

$$\begin{aligned}\nabla^{\gamma} v &= -\frac{1}{2\cos(\pi\gamma/2)}(D_{+}^{\gamma} v + D_{-}^{\gamma} v),\\ D_{+}^{\gamma} v &= \frac{1}{\Gamma(2-\gamma)}\frac{d^2}{dx^2}\int_{-\infty}^{x}\frac{v(\xi,t)}{(x-\xi)^{\gamma-1}}d\xi,\\ D_{-}^{\gamma} v &= \frac{1}{\Gamma(2-\gamma)}\frac{d^2}{dx^2}\int_{x}^{\infty}\frac{v(\xi,t)}{(\xi-x)^{\gamma-1}}d\xi,\end{aligned}$$

where $\Gamma(\cdot)$ stands for the Gamma function. It is verified that the Fourier transform of $\nabla^{\gamma} v$ satisfies $\mathcal{F}(\nabla^{\gamma} v) = -|k|^{\gamma}\mathcal{F}(v)$. In higher dimensions, the Laplacian is replaced by the operator $\nabla^{\gamma} = -(-\Delta)^{\gamma/2}$, defined by its action in Fourier space, $\mathcal{F}(\nabla^{\gamma} v) = -|\mathbf{k}|^{\gamma}\mathcal{F}(v)$.

The reaction term in system (2) was first given by Dufiet and Boissonade to describe the chlorite-iodine-malonic acid reaction [42]. Here a, b, and c are positive constants. The quadratic term uv avoids the invariance in the transformation $(u,v) \to (-u,-v)$ while the cubic term $-u^3$ limits the exponential growth of the perturbation and allows for the saturation of the instability. Dufiet and Boissonade [42] studied the dynamics of Turing pattern monolayers in system (2) with normal diffusion and found that monolayer Turing patterns arise from a transverse instability with a delay when compared to the genuine 2D systems.

The paper is structured as follows. In Sec. II by considering the linear stability of the steady state, we give the Turing parameter space to ensure that Turing bifurcation occurs prior to Hopf bifurcation. In Sec. III we present a weakly nonlinear analysis to derive a set of coupled amplitude equations. By analyzing these equations, we describe hexagonal and stripped patterns and their stability. Moveover, we find that the quadratic term can tune the mode of steady state. In Sec. IV we present the results of numerical computations. In addition to verifying the results of our analysis by computing hexagonal and striped patterns near the neutral stability boundaries, we also numerically explore the effects of distinct diffusion exponent between the two species on Turing pattern dynamics. Our paper closes with a brief discussion.

II. LINEAR STABILITY ANALYSIS

In this section, we derive the conditions for Turing bifurcation by analyzing the linear stability of the uniform equilibrium to the system (2). This system has three spatially uniform stationary states $(u_0,v_0) = (0,0)$, $(u_1,v_1)=(\frac{b+\sqrt{b^2+4(c-a)c}}{2c}, \frac{b+\sqrt{b^2+4(c-a)c}}{2c^2})$, and $(u_2,v_2) = (\frac{b-\sqrt{b^2+4(c-a)c}}{2c}, \frac{b-\sqrt{b^2+4(c-a)c}}{2c^2})$. When b is very small [i.e., $b < \sqrt{c(a-c)}$], the latter two equilibria exist only when the first equilibrium far surpasses the Turing bifurcation point. Thus we can ignore the existence of the latter two equilibria. In this paper, we only analyze the stability of the first equilibrium (u_0,v_0).

In the absence of diffusion, when $a > 1$ the spatially homogeneous system corresponding to the system (2) exhibits a Hopf bifurcation at $c = 1$. The equilibrium is stable to any small spatially homogeneous perturbation for $1 < c < a$. When the diffusion terms are present, we seek the general solution

$$\begin{pmatrix} u \\ v \end{pmatrix} = \begin{pmatrix} c_1 \\ c_2 \end{pmatrix} \exp(\sigma t + i\mathbf{k}\cdot\mathbf{r}) \tag{4}$$

to the linearization of system (2) as a superposition of normal modes. Here σ is the growth rate of the perturbation in time t. i is the imaginary unit and $i^2 = -1$. $\mathbf{k}$ is its wave vector, and $\mathbf{r}$ is the spatial vector. According to the definition of Weyl fractional operator ∇^{γ}, we can consider the time integration in Fourier space. Substituting Eq. (4) into the linearization of system (2), we obtain the following matrix equation:

$$\begin{pmatrix} \sigma - 1 + k^{\gamma} & a \\ -1 & \sigma + c + dk^{\gamma} \end{pmatrix} \begin{pmatrix} c_1 \\ c_2 \end{pmatrix} = \begin{pmatrix} 0 \\ 0 \end{pmatrix},$$

where the Euclidean norm $k = |\mathbf{k}|$ is the wave number of the perturbation. Therefore, we have to obtain the dispersion relation

$$\sigma^2 + g(k)\sigma + h(k) = 0, \tag{5}$$

where $g(k) = (1+d)k^{\gamma} - 1 + c$ and $h(k) = dk^{2\gamma} + (c-d)k^{\gamma} - c + a$.

The equilibrium can lose its stability both via Hopf and Turing bifurcation. Hopf instability occurs when $g(k) = 0$ for $k = 0$ and $h(k) > 0$. Then we can get the critical value of the Hopf bifurcation parameter c_H,

$$c_H = 1.$$

The system (2) undergoes Turing bifurcation if and only if $h(k) \leqslant 0$. $h(k)$ has a single minimum at (k_c,a_c), where

$$k_c = \left(\frac{d-c}{2d}\right)^{\frac{1}{\gamma}}, \quad a_c = \frac{(d+c)^2}{4d}. \tag{6}$$

In conclusion, we obtain the Turing instability threshold a_c and the critical value of the wave number k_c. Moreover, in order for Turing bifurcation to occur prior to oscillatory instability

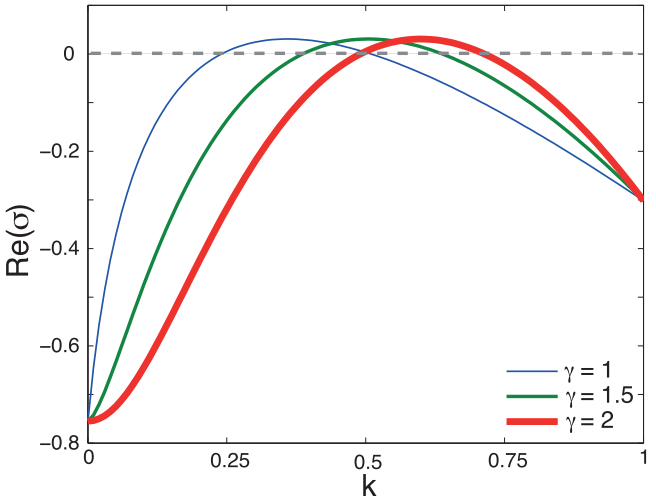

FIG. 1. (Color online) Dispersion relation of the system (2) for three different $\gamma = 1,1.5,2$. $\gamma = 2$ represents the normal diffusion. Other parameters are $a = 7.45$, $b = 2.5$, $c = 5$, and $d = 20$.

as a decreases, we need the following Turing instability's parameter space:

$$1 < c < a < a_c, \quad d > 1, \quad b < \sqrt{c(a-c)}, \tag{7}$$

such that the system is stable to any small spatially homogeneous perturbation.

In Fig. 1 we show the real part of the eigenvalue corresponding to three different sets of parameters as a function of the wave number. The superdiffusive exponent γ plays an important role in the active wave number, which increases with γ.

III. WEAKLY NONLINEAR ANALYSIS AND PATTERN SELECTION

In this section we confine the system (2) into the two-dimensional spatial domain $\mathbb{R}^2$ to study the dynamics of Turing pattern by performing a weakly nonlinear analysis of the system (2) near the Turing instability threshold. In particular, we aim to study the pattern selection of hexagons and stripes. The weakly nonlinear analysis is based on the fact that Turing bifurcation destabilizes the homogeneous equilibrium only in regard to perturbation with wave numbers close to the critical value k_c. Close to Turing onset $a = a_c$, the solutions can be described by a system of three active resonant pairs of modes $(\mathbf{k}_j, -\mathbf{k}_j)$ $(j = 1,2,3)$. Here each mode makes angles of $2\pi/3$ and $\mathbf{k_j} = k_c$. Thus the solutions of the system (2) can be expanded as

$$\begin{pmatrix} u \\ v \end{pmatrix} = \sum_{j=1}^{3} [\mathbf{A}_j \exp(i\mathbf{k}_j \cdot \mathbf{r}) + \bar{\mathbf{A}}_j \exp(-i\mathbf{k}_j \cdot \mathbf{r})], \tag{8}$$

where $\mathbf{A}_j$ and the conjugate $\bar{\mathbf{A}}_j$ are, respectively, the amplitudes associated with the modes $\mathbf{k}_j$ and $-\mathbf{k}_j$, and $\mathbf{A}_j \equiv (A_j^u, A_j^v)^T$.

We introduce the slow time $T = \varepsilon^2 t$ and expand both u and v as well as the bifurcation parameter a as

$$\begin{pmatrix} u \\ v \end{pmatrix} = \varepsilon \begin{pmatrix} u_1 \\ v_1 \end{pmatrix} + \varepsilon^2 \begin{pmatrix} u_2 \\ v_2 \end{pmatrix} + \varepsilon^3 \begin{pmatrix} u_3 \\ v_3 \end{pmatrix} + \cdots,$$
$$a_c - a = \mu_2 \varepsilon^2 + O(\varepsilon^3). \tag{9}$$

As the amplitude $\mathbf{A}$ is a variable that changes slowly, then we have

$$\frac{\partial \mathbf{A}}{\partial t} = \varepsilon^2 \frac{\partial \mathbf{A}}{\partial T} + O(\varepsilon^3). \tag{10}$$

Substituting Eqs. (9) into the system (2) and collecting like powers of ε, we obtain, at orders $\varepsilon^j (j = 1,2,3)$, the sequences of equations as follows:

$$O(\varepsilon): \mathbf{L_c} \begin{pmatrix} u_1 \\ v_1 \end{pmatrix} = 0,$$
$$O(\varepsilon^2): \mathbf{L_c} \begin{pmatrix} u_2 \\ v_2 \end{pmatrix} = \begin{pmatrix} -bu_1 v_1 \\ 0 \end{pmatrix},$$
$$O(\varepsilon^3): \mathbf{L_c} \begin{pmatrix} u_3 \\ v_3 \end{pmatrix} = \frac{\partial}{\partial T} \begin{pmatrix} u_1 \\ v_1 \end{pmatrix} + \begin{pmatrix} -\mu_2 v_1 - b(u_1 v_2 + u_2 v_1) + u_1^3 \\ 0 \end{pmatrix}, \tag{11}$$

where

$$\mathbf{L_c} = \begin{pmatrix} 1 + \nabla^\gamma & -a_c \\ 1 & -c + d\nabla^\gamma \end{pmatrix}. \tag{12}$$

We wish to describe the appearance of both hexagons and stripes as well as their interactions. Since $\mathbf{L_c}$ is the linear operator of the system at the Turing instability threshold, $(u_1, v_1)^T$ is the linear combination of the eigenvectors corresponding to the eigenvalue 0. Therefore, at $O(\varepsilon)$ the solution is given in the form

$$\begin{pmatrix} u_1 \\ v_1 \end{pmatrix} = \begin{pmatrix} (c+d)/2 \\ 1 \end{pmatrix} \sum_{j=1}^{3} W_j \exp(i\mathbf{k}_j \cdot \mathbf{r}) + \text{c.c.},$$

where W_j is the amplitude of the mode $\exp(i\mathbf{k}_j \cdot \mathbf{r})$ when the system is under the first-order perturbation. Its form is determined by the perturbational term of the higher order.

Next, we turn to the $O(\varepsilon^2)$ problem. Since the right-hand side does not have the resonance, the solution is given by the form

$$\begin{pmatrix} u_2 \\ v_2 \end{pmatrix} = \begin{pmatrix} U_0 \\ V_0 \end{pmatrix} + \begin{pmatrix} U_j \\ V_j \end{pmatrix} \sum_{j=1}^{3} \exp(i\mathbf{k}_j \cdot \mathbf{r}) + \text{c.c}$$

Substituting the above equation into the second equation of the problem (11), we have

$$\begin{pmatrix} U_0 \\ V_0 \end{pmatrix} = \frac{4bd(c+d)\Sigma_{j=3}^{3} |W_j|^2}{(c-d)^2} \begin{pmatrix} c \\ 1 \end{pmatrix},$$
$$U_j = \frac{c+d}{2} V_j. \tag{13}$$

We now turn to the $O(\varepsilon^3)$ problem. According to the Fredholm solubility condition, the vector function of the right-hand side must be orthogonal with the zero eigenvalues of the operator $\mathbf{L}_\mathbf{c}^+$ to ensure the existence of the nontrivial solution to this equation, where $\mathbf{L}_\mathbf{c}^+$ is the adjoint operator of $\mathbf{L}_\mathbf{c}$. The nontrivial kernel of the operator $\mathbf{L}_\mathbf{c}^+$ is

$$\begin{pmatrix} 1 \\ -(c+d)/2d \end{pmatrix} \exp(-i\mathbf{k}_j \cdot \mathbf{r}), \quad j = 1,2,3. \tag{14}$$

Substituting the solution $(u_1, v_1)^T$ and $(u_2, v_2)^T$ into the $O(\varepsilon^3)$ problem and using the Fredholm solubility condition, we have

$$\begin{aligned} &\frac{(d-1)(c+d)}{2d}\frac{\partial W_1}{\partial T} \\ &= \mu_2 W_1 + b(c+d)(\bar{W}_2\bar{V}_3 + \bar{V}_2\bar{W}_3) \\ &\quad - \left[\frac{3(c+d)^3}{8}|W_1|^2 + \frac{3(c+d)^3}{4}(|W_2|^2 + |W_3|^2)\right] W_1. \end{aligned} \tag{15}$$

The other two equations of W_2 and W_3 can be obtained through the transformation of the subscript of W. In view of Eqs. (8) and (9), the amplitude $A_j^u = \frac{c+d}{2} A_j^v$ can be expanded as

$$\begin{aligned} A_j^u &= \frac{c+d}{2}[\varepsilon W_j + \varepsilon^2 V_j + O(\varepsilon^3)], \quad (j = 1,2,3), \\ \frac{\partial A_j^u}{\partial t} &= \varepsilon^3 \frac{c+d}{2}\frac{\partial W_j}{\partial T} + O(\varepsilon^4). \end{aligned} \tag{16}$$

Multiplying Eq. (15) by ε^3, we get

$$\begin{aligned} \frac{d-1}{d}\frac{\partial A_1^u}{\partial t} &= \frac{2(a_c - a)}{c+d} A_1^u + \frac{4b}{c+d}\bar{A}_2^u \bar{A}_3^u \\ &\quad - m\left[3\left|A_1^u\right|^2 + 6\left(\left|A_2^u\right|^2 + \left|A_3^u\right|^2\right)\right] A_1^u. \end{aligned} \tag{17}$$

Multiplying Eq. (17) by $\frac{2d}{c+d}$ and using $a_c = \frac{(d+c)^2}{4d}$, we have the amplitude equation

$$\begin{aligned} \tau_0 \frac{\partial A_1^u}{\partial t} &= \mu A_1^u + h\bar{A}_2^u \bar{A}_3^u \\ &\quad - \left[g_1\left|A_1^u\right|^2 + g_2\left(\left|A_2^u\right|^2 + \left|A_3^u\right|^2\right)\right] A_1^u, \end{aligned} \tag{18}$$

where $\mu = \frac{a_c - a}{a_c}$ is a normalized distance to the Turing instability threshold, and $\tau_0 = \frac{2(d-1)}{c+d}$ is a typical relaxation time. Moreover,

$$h = \frac{8bd}{(c+d)^2}, \quad g_1 = \frac{6d}{c+d}, \quad g_2 = \frac{12d}{c+d}. \tag{19}$$

Similar equations for A_2^u and A_3^u are obtained by circular permutation of indices.

From the amplitude equation (18), the coefficient of second order is far smaller than that of third order for $d > 1$. Since the coefficients of third order are negative, the saturation of the instability is achieved at third order. Therefore, these amplitude equations are valid, and Turing bifurcation is supercritical.

In order to study the pattern selection, we need to further analyze the amplitude equation (18). Since the supercritical Turing bifurcation implies that the solutions to the amplitude equation (18) are stable, the dynamics of Turing patterns are asymptotically stable. In Eq. (18), each amplitude can be decomposed to mode $\rho_j = |A_j^u|$ and a corresponding phase angle φ_j. We rewrite Eq. (18) and the associated other two amplitude equations by $A_j^u = \rho_j \exp(i\varphi_j)$ in the form

$$\begin{aligned} \tau_0 \frac{\partial \Phi}{\partial t} &= -h\frac{\rho_1^2\rho_2^2 + \rho_1^2\rho_3^2 + \rho_2^2\rho_3^2}{\rho_1\rho_2\rho_3}\sin\Phi, \\ \tau_0 \frac{\partial \rho_1}{\partial t} &= \mu\rho_1 + h\rho_2\rho_3\cos\Phi - g_1\rho_3 - g_2\left(\rho_2^2 + \rho_3^2\right)\rho_1, \\ \tau_0 \frac{\partial \rho_2}{\partial t} &= \mu\rho_2 + h\rho_1\rho_3\cos\Phi - g_1\rho_2 - g_2\left(\rho_1^2 + \rho_3^2\right)\rho_2, \\ \tau_0 \frac{\partial \rho_3}{\partial t} &= \mu\rho_3 + h\rho_1\rho_2\cos\Phi - g_1\rho_3 - g_2\left(\rho_1^2 + \rho_2^2\right)\rho_3, \end{aligned} \tag{20}$$

where $\Phi = \phi_1 + \phi_2 + \phi_3$.

After a standard stability analysis of Eqs. (20) as in [43–46], we obtain that the steady state possibly possesses five kinds of solutions: homogeneous steady state $[O(1)]$, striped pattern B $(\rho_1 \neq 0, \rho_2 = \rho_3 = 0)$ (e.g., Fig. 4), hexagonal patterns H_0 (e.g., Fig. 3) or H_π $(\rho_1 = \rho_2 = \rho_3 \neq 0$, with $\Phi = 0$ or π, respectively), and a mixed state (e.g., Fig. 5). Patterns H_0 (positive hexagon) and H_π (negative hexagon) differ in whether the minima or maxima are disposed on the hexagonal lattice. Their existence and stability limits, as a function of the scaled bifurcation parameter μ, are ordered according to the general bifurcation diagram as in [42], where μ_i are given by

$$\begin{aligned} \mu_1 &= -\frac{8b^2 d}{15(c+d)^3}, \quad \mu_2 = 0, \\ \mu_3 &= \frac{32b^2 d}{3(c+d)^3}, \quad \mu_4 = \frac{128b^2 d}{3(c+d)^3}. \end{aligned} \tag{21}$$

According to the pattern selection theory of [42], the system exists in the bistable state between the hexagon and the stripe only if the control parameter μ lies in the range $\mu_3 < \mu < \mu_4$, or equivalently the quadratic coefficient b locates in $b_2 < b < b_3$, where

$$b_2 = \frac{\sqrt{6}}{16}\frac{(c+d)^3 - 4ad(c+d)}{d}, \quad b_3 = 2b_2. \tag{22}$$

When $b = 0$, the nongeneric symmetry $(u, v) \to (-u, -v)$ is restored. In this case, the striped pattern bifurcates supercritically whereas the stability range of the hexagonal pattern vanishes. Therefore, when Turing bifurcation emerges, we can choose b as the control parameter to tune the type of steady state.

Figure 2 demonstrates a schematic diagram of pattern selection. When the control parameter b lies in $0 < b < b_2$, stripped pattern is stable, and both the positive and negative hexagonal pattern are unstable. In the range $b_2 < b < b_3$, the system (2) exists in a bistable state between positive hexagonal and striped patterns; for $b > b_3$, striped pattern loses its stability and the positive hexagon is stable.

IV. NUMERICAL SIMULATIONS

For numerical study of pattern formation in the system (2), we only need consider the dynamics of the perturbation to the spatially homogeneous steady state. Hence we use the periodic boundary conditions and the small-amplitude random initial data to the system (2). We can use the pseudospectral method

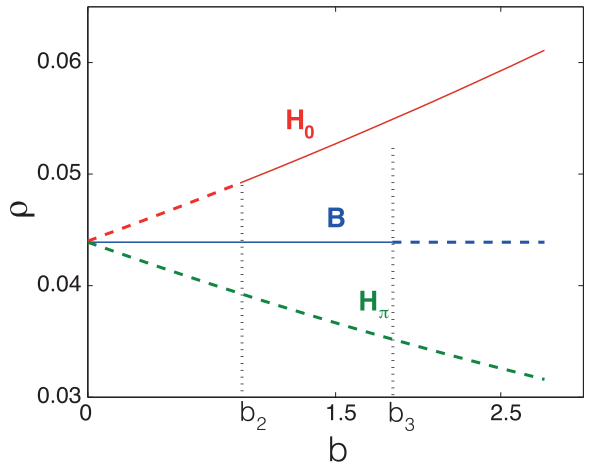

FIG. 2. (Color online) Bifurcation diagram of Turing patterns, in the (b,ρ) plane, of the system (2). H_0 is the positive hexagonal patterns with $\Phi = 0$; H_π is the negative hexagonal patterns with $\Phi = \pi$; B is the striped patterns. The other parameters are $a = 7.45$, $c = 5$, $d = 20$, and $\gamma = 1.5$. Here the critical values $b_2 = 0.9217$ and $b_3 = 1.8435$. The solid lines represent stable states. The dashed lines represent unstable states.

[47] to perform numerical computations with time integration in Fourier space. Moreover, we use a Crank-Nicolson scheme for the linear operator and an Adams-Bashforth scheme for the nonlinear operator [48].

Our numerical computations first confirm the effects of the order γ of Weyl fractional operator on the wave number of Turing patterns. Figure 3 shows that when γ decreases from 2 to 1, the wave number of Fig. 3(a) is more than that of Fig. 3(b), which is also in accordance with Fig. 1.

We now verify the Turing bifurcation diagram (Fig. 2), which is obtained by means of the weakly nonlinear analysis. In Fig. 4, we take the control parameter as $b = 0.5$, which satisfies $b < b_2 = 0.9217$. The steady state first breaks up into the hexagons due to initially introduced small perturbation [Fig. 4(a)]. The emergent hexagons are not stable and replaced gradually by stripes [Figs. 4(b) and 4(c)]. Eventually, the stripes prevail over the whole domain, and the dynamics of the system does not undergo any further changes. Interestingly, we notice that the directions of the stripes is sensitive to initial values and horizontal strips can also be possible with other appropriate initial conditions.

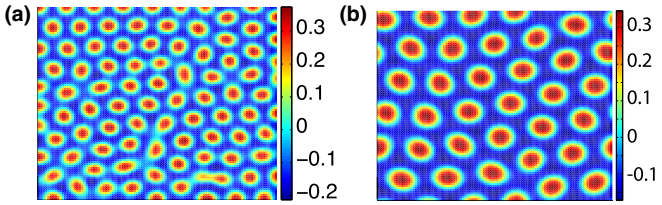

FIG. 3. (Color online) Turing patterns for different orders of Weyl fractional operator. (a) $\gamma = 2$ (i.e., normal diffusion), (b) $\gamma = 1$ (superdiffusion). The other parameters are $a = 7.45$, $b = 2.5$, $c = 5$, $d = 20$.

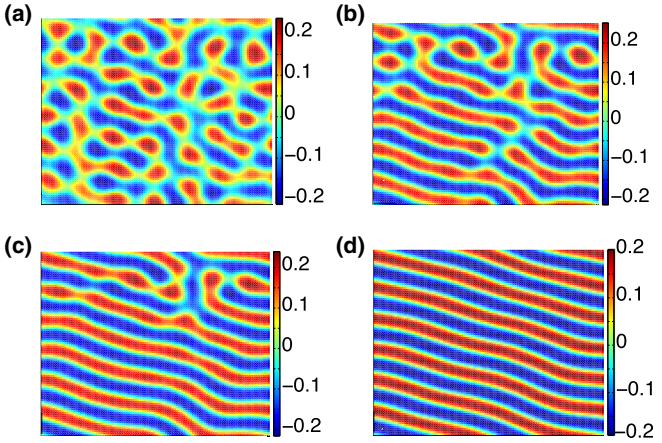

FIG. 4. (Color online) Snapshots of stable stripes at different time (control parameter $b = 0.5$). (a) $t = 150$, (b) $t = 300$, (c) $t = 450$, (d) $t = 1000$. The other parameters are $a = 7.45$, $c = 5$, $d = 20$, and $\gamma = 1.5$.

When the control parameter $b = 1.5$ locates in the range (b_2,b_3), the hexagons first occur [Fig. 5(a)]. Then some hexagons are gradually replaced by stripes, while the remaining do not change [Figs. 5(b) and 5(c)]. Ultimately, both the hexagonal patterns and the striped patterns coexist [Fig. 5(d)], which exhibits a bistable regime. When the control parameter $b = 2.5$ lies in the range $b > b_3 = 1.8435$, the pattern dynamics converges to stable hexagonal patterns (Fig. 6).

So far we have considered spatial patterns in system (2) for the case where the activator and inhibitor have the same superdiffusive exponent (i.e., γ). An interesting question is how different superdiffusive exponents impact the emergent spatial patterns. To this end, we take Fig. 5 as a reference (i.e., control parameter $b = 1.5$) and explore this question numerically. Figure 7 clearly demonstrates that there is a qualitative change when the activator and inhibitor have different superdiffusive exponents. When the activator has a larger superdiffusive

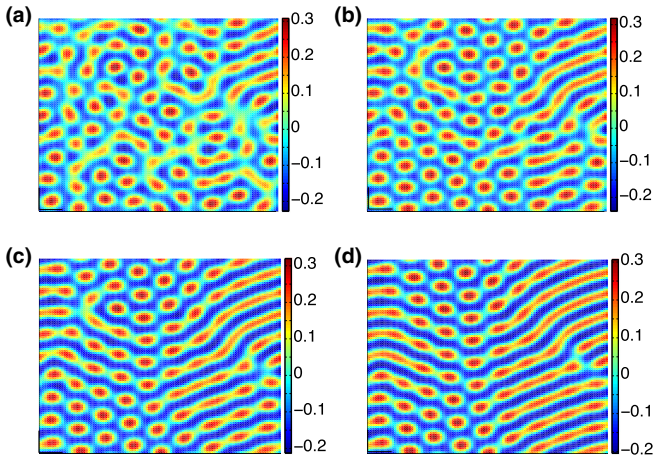

FIG. 5. (Color online) Snapshots of the coexistence of strips and hexagons at different time (control parameter $b = 1.5$). (a) $t = 150$, (b) $t = 350$, (c) $t = 600$, (d) $t = 1000$. Other parameters are the same as in Fig. 4.

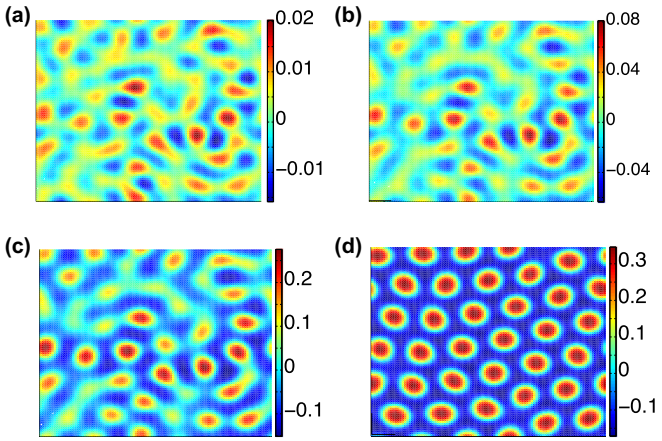

FIG. 6. (Color online) Snapshots of stable hexagonal patterns at different time (control parameter $b = 2.5$). (a) $t = 50$, (b) $t = 100$, (c) $t = 150$, (d) $t = 1000$. Other parameters are the same as in Fig. 4.

exponent than the inhibitor, a striped pattern appears, and when the opposite is true, hexagons coexist with stripes. All emergent spatial patterns are stationary. Furthermore, in each region, there is only quantitative change in the emergent spatial patterns due to the decreased wave number with increased γ (Fig. 1).

As the diffusion rates manifest in both a diffusion constant and a diffusion exponent, we now explore how the diffusion ratio interacts with the diffusion exponent to govern the formation of spatial patterns. Figure 8 shows that for a given diffusion exponent of the activator, the critical ratio of diffusion constant (i.e., d) required for Turing patterns to occur increases with the diffusion exponent of the inhibitor. This explains why the patterns displayed in the upper left corner of Fig. 7 occur with high diffusion ratio.

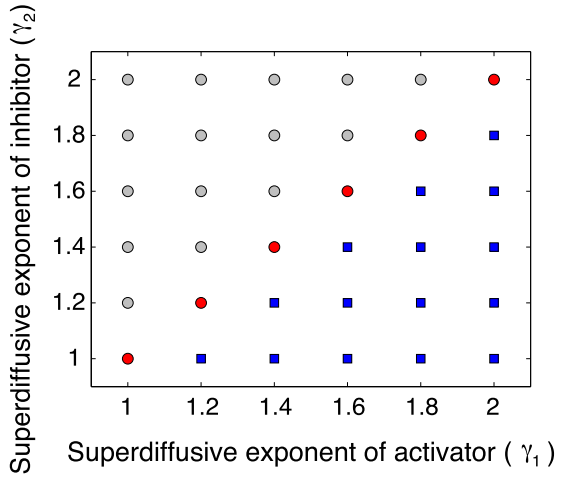

FIG. 7. (Color online) Pattern diagram for different combinations of the superdiffusive exponents of activator and inhibitor, denoted by γ_1 and γ_2, respectively. Blue squares indicate striped patterns [e.g., Fig. 4(d)], while cycles indicate mixed patterns of stripes and hexagons [e.g., Fig. 5(d)]. Parameters are $a = 7.45$, $b = 1.5$, $c = 5$, and $d = 20$. The diffusion ratio (i.e., d) for the grey circles is greater than 20 to drive the emergence of spatial patterns.

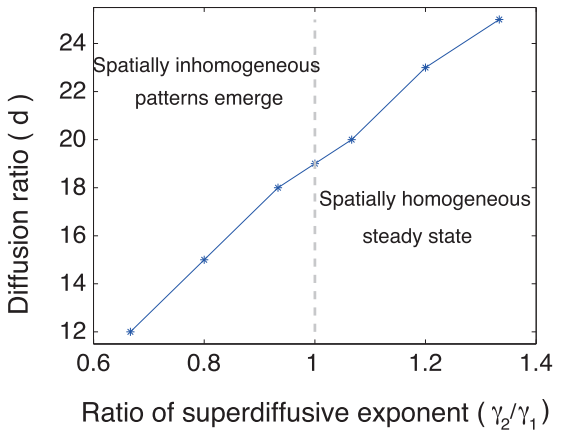

FIG. 8. (Color online) The minimum diffusion constant ratio (i.e., d) for the formation of Turing patterns varies with the ratio of the superdiffusive exponent of the inhibitor to the activator (solid line). Spatial pattern arises above the solid line. To the left (right) of the dashed line, the inhibitor has smaller (lager) superdiffusive exponent than the activator. Parameters are $a = 7.45$, $b = 1.5$, $c = 5$, $d = 20$, and $\gamma_1 = 1.5$.

V. DISCUSSION

We have introduced the Lévy flights type of superdiffusion into an activator-inhibitor system to describe species' anomalous diffusion. Linear stability analysis showed that the superdiffusive exponent (i.e., γ) has an important effect on the wave number of Turing patterns. Our weakly nonlinear analysis revealed that the coefficient of the quadratic term can tune the modes of the steady state, which is in accordance with the observations in the normal diffusion model [42]. Moreover, we found that different superdiffusive exponents of the activator and inhibitor lead to both qualitative and quantitative changes in emergent spatial patterns. Finally, we showed that the critical value of the diffusion ratio (i.e., d) for Turing instability to occur increases with the diffusion exponent ratio of inhibitor to activator, and this finding is robust, independent of the specified diffusion exponent of the activator that was used in Fig. 8. In addition, if the activator experiences superdiffusion while the inhibitor has normal diffusion, we found that a larger diffusion ratio is required to trigger the emergence of the Turing pattern, compared to the case where both species have normal diffusion.

Lévy flights are stochastic process characterized by the occurrence of extremely long jumps such that the same sites are revisited much less frequently than in a normal diffusion process. The length of these jumps is distributed according to Lévy stable statistics with a power-law tail and divergence of the second moment, which strongly contradicts the ordinary Brownian motion for which all moments of the particle coordinate are finite. The power-law tail is also termed as "fat-tailed distribution" because the tail falls off much more gently than for a Gaussian distribution. It is the property that lies at the heart of the interesting and unusual behavior of Lévy flights. Realization of the Lévy flights in physical phenomena are very diverse such as in fluid dynamics, dynamical systems, and micelles [49,50]. Recent field study in ecology provided convincing evidence for the existence of

Lévy flights among the foraging of marine predators ranging across natural landscapes [51,52]. It was found that Lévy flights are expected in places where prey is scare (e.g., less productive waters such as the open ocean) while Brownian strategy is more likely to occur where prey is abundant (e.g., the productive shelf or convergence-front habitats). These two foraging strategies can be alternately performed by some individuals and which is the ongoing strategy depends on the gradients of environment that the individuals are involved in.

Here we considered a very basic but generic chemical problem, and how the achieved results can be used to understand population dynamics and foraging strategies in ecology remains unclear. An interesting ecological question is if Lévy flights can promote the survival of populations through optimizing random search in the period of food scarcity. Another interesting and promising future work is how to experimentally control the anomalous diffusion exponent in superdiffusive reaction-diffusion systems such that we can understand if animals will evolve to exploit a Lévy foraging strategy. In a chemical system where superdiffusion is caused by turbulent mixing, a possible way to control the anomalous exponents would be to vary the mixing intensity [53].

ACKNOWLEDGMENTS

L.Z. gratefully acknowledges the financial support from the Swedish Strategic Research Programme eSSENCE. C.T. acknowledges partial support by the National Natural Science Foundation of China No. NSFC 11201406, and the Qinglan Project.

[1] A. Turing, Philos. Trans. R. Soc. London, Ser. B **237**, 37 (1952).
[2] S. A. Levin and L. A. Segel, Nature **259**, 659 (1976).
[3] L. A. Segel and J. L. Jackson, J. Theor. Biol. **37**, 545 (1972).
[4] M. Baurmann, T. Gross, and U. Feudel, J. Thoer. Biol. **245**, 220 (2007).
[5] Y. Astrov, E. Ammelt, S. Teperick, and H. G. Purwins, Phys. Lett. A **211**, 184 (1996).
[6] H. Nakoa and A. S. Mikhailov, Nat. Phys. **6**, 544 (2010).
[7] P. Liang, Phys. Rev. Lett. **75**, 1863 (1995).
[8] F. T. Arecchi, S. Boccaletti, and P.-L. Ramazza, Phys. Rep. **318**, 1 (1999).
[9] K. Staliunas and V. J. Snchez-Morcillo, Opt. Commun. **177**, 389 (2000).
[10] J. D. Murray, *Mathematical Biology II: Spatial Models and Biomedical Applications* (Springer-Verlag, New York, 2003).
[11] T. Shin, D. Kraemer, J. Pryor, L. Liu, J. Rugila, L. Howe, S. Buck, K. Murphy, L. Lyons, and M. Westhusin, Nature **415**, 859 (2002).
[12] J. P. Bouchard and A. Georges, Phys. Rep. **195**, 127 (1990).
[13] R. Metzler and J. Klafter, Phys. Rep. **339**, 1 (2000).
[14] R. Metzler and J. Klafter, J. Phys. A **37**, R161 (2004).
[15] I. M. Sokolov, J. Klafter, and A. Blumen, Phys. Today **55**, 48 (2002).
[16] A. Golovin, B. Matkowsky, and V. Volpert, SIAM J. Appl. Math. **69**, 251 (2008).
[17] G. Gambino, M. C. Lombardo, and M. Sammartino, Phys. Rev. E **88**, 042925 (2013).
[18] A. E. Hansen, D. Marteau, and P. Tabeling, Phys. Rev. E **58**, 7261 (1998).
[19] T. H. Solomon, E. R. Weeks, and H. Swinney, Phys. Rev. Lett. **71**, 3975 (1993).
[20] J. M. Sancho, A. M. Lacasta, K. Lindenberg, I. M. Sokolov, and A. H. Romero, Phys. Rev. Lett. **92**, 250601 (2004).
[21] G. M. Viswanathan, V. Afanasyev, S. V. Buldyrev, E. J. Murphy, P. A. Prince, and H. E. Stanley, Nature **381**, 413 (1996),
[22] F. G. Schmitt and L. Seuront, Physica A **301**, 375 (2001).
[23] J. Toner, Y. Tu, and S. Ramaswamy, Ann. Phys. (NY) **318**, 170 (2005).
[24] M. Weiss, Phys. Rev. E **68**, 036213 (2003).
[25] G. Drazer and D. H. Zanette, Phys. Rev. E **60**, 5858 (1999).
[26] F. Amblard, A. C. Maggs, B. Yurke, A. N. Pargellis, and S. Leibler, Phys. Rev. Lett. **77**, 4470 (1996).
[27] V. V. Gafiychuk and B. Y. Datsko, Physica A **365**, 300 (2006).
[28] B. I. Henry, T. A. M. Langlands, and S. L. Wearne, Phys. Rev. E **72**, 026101 (2005).
[29] B. I. Henry and S. L. Wearne, SIAM J. Appl. Math. **62**, 870 (2002).
[30] T. A. M. Langlands, B. I. Henry, and S. L. Wearne, J. Phys. Condens. Matter **19**, 065115 (2007).
[31] M. Weiss, H. Hashimoto, and T. Nilsson, Biophys. J. **84**, 4043 (2003).
[32] B. W. Li and J. Wang, Phys. Rev. Lett. **91**, 044301 (2003).
[33] Y. Nec, A. A. Nepomnyashchy, and A. A. Golovin, Europhys. Lett. **82**, 58003 (2008).
[34] V. K. Vanag, Physics-Uspekhi **47**, 923 (2004).
[35] G. M. Viswanathan, S. V. Buldyrev, S. Havlin, M. G. E. da Luz, E. P. Raposo, and H. E. Stanley, Nature **401**, 911 (1999).
[36] D. W. Sims, A. M. Reynolds, N. E. Humphries, E. J. Southall, V. J. Wearmouth, B. Metcalfe, and R. J. Twitchettf, Proc. Natl Acad. Soc. USA **111**, 11073 (2014).
[37] M. M. Meerschaert, J. Mortensen, and S. W. Wheatcraft, Physica A **367**, 181 (2006).
[38] P. Lévy, *Théorie de l'Addition des Variables Aléatoires* (Gauthier, Paris, 1954).
[39] A. Chaves, Phys. Lett. A **239**, 13 (1998).
[40] D. A. Benson, S. W. Wheatcraft, and M. M. Meerschaert, Water Resource Res. **36**, 1413 (2000).
[41] M. M. Meerschaert, D. A. Benson, H.-P. Scheffler, and B. Baeumer, Phys. Rev. E **65**, 041103 (2002).
[42] V. Dufiet and J. Boissonade, Phys. Rev. E **53**, 4883 (1996).
[43] G. H. Gunaratne, Q. Ouyang, and H. L. Swinney, Phys. Rev. E **50**, 2802 (1994).
[44] Q. Ouyang, *Nonlinear Science and Introduction of Pattern Dynamics* (Beijing University Press, Beijing, 2010).
[45] W. Wang, Q. X. Liu, and Z. Jin, Phys. Rev. E **75**, 051913 (2007).
[46] X. C. Zhang, G. Q. Sun, and Z. Jin, Phys. Rev. E **85**, 021924 (2012).
[47] W. Huang and D. M. Sloan, J. Comput. Phys. **111**, 399 (1994).
[48] Y. He and W. Sun, SIAM J. Numer. Anal. **45**, 837 (2007).

[49] M. G. Shlesinger, G. M. Zaslavsky, and J. Klafter, Nature **363**, 31 (1993).
[50] M. G. Shlesinger, G. M. Zaslavsky, and U. Frisch, *Lévy Flights and Related Topics in Physics* (Springer, Berlin, 1995).
[51] N. E. Humphries, N. Queiroz, J. R. M. Dyer *et al.*, Nature **465**, 1066 (2010).
[52] G. M. Viswanathan, Nature **465**, 1018 (2010).
[53] B. Zhao and J. Wang, J. Phys. Chem. A **109**, 3647 (2005).